Novel method to achieve crystallinity of calcite by *Bacillus subtilis* in coupled and non-coupled calcium-carbon sources

Héctor Ferral-Pérez
Universidad Autonoma de Ciudad Juarez
Mónica Galicia-García
Universidad Autonoma de Ciudad Juarez
Bonifacio Alvarado-Tenorio
Universidad Autonoma de Ciudad Juarez
Aldo Izaguirre-Pompa
Universidad Autonoma de Ciudad Juarez
Marisela Aguirre-Ramírez (marisela.aguirre@uacj.mx)
Universidad Autonoma de Ciudad Juarez https://orcid.org/0000-0002-9764-0324

Original article

Keywords: Bacillus subtilis organomineralization, biogenic calcite, calcium carbonate composites, micrite

Posted Date: September 10th, 2020

DOI: https://doi.org/10.21203/rs.3.rs-70717/v1

Version of Record: A version of this preprint was published at AMB Express on September 29th, 2020. See the published version at https://doi.org/10.1186/s13568-020-01111-6.

Abstract

Bacteria mineralization is a promising biotechnological approach to apply in biomaterials development. In this investigation, we demonstrate that *Bacillus subtilis* 168 induces and influences $CaCO_3$ composites precipitation. Crystals were formed in calcium-carbon non-coupled (glycerol + $CaCl_2$, GLY; or glucose + $CaCl_2$, GLC) and coupled (calcium lactate, LAC; or calcium acetate, ACE) agar-sources, only maintaining the same Ca^{2+} concentration. The mineralized colonies showed variations in morphology, size, and crystallinity form properties. The crystals presented spherulitic growth in all conditions, and botryoidal shapes in GLC one. Birefringence and diffraction patterns confirmed that all biogenic carbonate crystals (BCC) were organized as calcite. The $CaCO_3$ in BCC was organized as calcite, amorphous calcium carbon (ACC) and organic matter (OM) of biofilm; all of them with relative abundance related to bacteria growth condition. BCC-GLY presented greatest OM composition, while BCC-ACE highest $CaCO_3$ content. Nucleation mechanism and OM content impacted in BCC crystallinity.

Key Points

- *B. subtilis* mineralized colonies show spherulitic and botryoidal growth.
- BCC are mainly composed for calcite, ACC and $CaCO_3$ precipitant wrapped up in EPS.
- Crystalitte is evident in non-coupled calcium-carbon sources conditions.

Introduction

Bacterial $CaCO_3$ mineralization is a phenomenon that occurs in sediments, caves, hot springs, soils and even in monuments and buildings (Ciferri et al. 2000; Rusznyák et al. 2012; Páramo et al. 2015). In nature, calcium carbonate biomineralization occurred in three different pathways: i) controlled biological mineralization (CBM), ii) induced biological mineralization (INDBM) and iii) influenced biological mineralization (INFBM) (Dove et al. 2003). In CBM, organisms produce ordered mineral structures by a specified enzymatic mechanism encoded in their genes (Ngwenya 2016). Moreover, INDBM and INFBM are passive mechanisms, where physiological activity induces spontaneous precipitation of ions (Knorre and Krumbein 2000) or mineralization are influenced by extracellular polymeric substances (EPS) and biofilm geometry (Dupraz et al. 2009), respectively. $CaCO_3$ precipitation is strongly influenced by basically four conditions: high pH environment (pK_2 [CO] = 10.3 at 25º C), oversaturation of Ca^{2+} and CO_3^{2-}, and availability of nucleation sites (Dupraz et al. 2009).

It has been demonstrated the occurrence of *B. subtilis* culture alkalinization in rich media (Robinson 1991) probably due to spontaneous extracellular proteins, or amino acids deamination (Dupraz et al. 2009). Besides, when cells oxidate the carbon sources, the resulting product comprises CO_2 and water. Under alkaline conditions, CO_2 (pK_2 [CO] = 10.3 at 25º C) spontaneously evolve into CO_3^{-2} (Stumm

1990). In addition, some *Bacillus* species could accelerate the hydration of CO_2(g) through carbonic anhydrase activity (Dhami et al. 2014).

Additionally, calcium uptake and extrusion in bacteria are passive processes promoted by osmotic forces across a Ca^{2+}/H^+ antiporter protein. Besides, there is a Ca^{+2}/Na^+ antiporter pump that also maintains low intracellular calcium concentration (De Vrij et al. 1985) and, creates a high saturated microenvironment near to cell wall and EPS (Banks et al. 2010; Perito and Mastromei 2011; Meier et al. 2017).

Finally, *B. subtilis* produced $CaCO_3$ minerals by INFBM; where EPS, membrane, and cell wall structurers act as nucleation sites (Perito et al. 2014; Priya et al. 2016). Specifically, the metabolism of fatty acids plays a key role in biomineralization process (Perito et al. 2000; Barabesi et al. 2007), such as dipicolinic acid (Marvasi et al. 2017).

In vitro, *B. subtilis* promotes calcite crystals formation in presence of different calcium sources such as calcium lactate (Sierra-Beltran et al. 2014), calcium acetate (Shirakawa et al. 2011) or calcium chloride (Shirakawa et al. 2011; Micallef et al. 2016). In most of those cases, the addition of urea to promote pH increase is recurrent. Nevertheless, a recent work shows that non-ureolityc *Bacillus* strains that precipitates calcite could be used to mortar healing (Reeksting et al. 2020).

In order to propose an alternative white biotechnology method, this research demonstrated that *B. subtilis* facilitates $CaCO_3$ precipitation through non-ureolytic pathway. As well, the acquiring of different crystallinity biogenic calcite could be achieved using either coupled or non-coupled calcium-carbon sources.

Material And Methods

Calcium carbonate biogenic crystal production and recovery

Bacillus subtilis 168 (ATCC®27370™) strain was used in this work. Bacteria pre-culture was propagated in Nutrient broth (BD Bioxon, Cuatitlán Izcalli, México) by 24 h, at 37 °C. Petri dishes with of four different agar composition were inoculated with 1.17×10^7 cells/ml. The plates were incubated at 37 ºC for 9 days. Nutrient Agar (BD Bioxon, Cuatitlán Izcalli, México) medium was supplemented with 0.026 M glycerol (Bio Basic, San Nicolas de la Garza, México) + 0.1M $CaCl_2$ (GLY), 0.013 M glucose (HYCEL, Zapopan, México) + 0.1M $CaCl_2$ (Jalmek, San Nicolás de la Garza, México) (GLC), 0.1 M calcium lactate (Cosmopólita, Naucalpan de Juárez, México) (LAC) or 0.1 M calcium acetate (LABESSA, Ciudad de México, México) (ACE). Bacteria growth modified pH values in liquid Nutrient Broth in all supplemented conditions. Initial pH varied between 6.5 to 7.1, and after eight hours, it increased until 9.3 as expected (Fig. S1).

After incubation time, to detach the mineralized colonies from agar, culture was washed (López-Moreno et al. 2014) with 5 mL of boiling water, for calcium acetate and calcium lactate media, 2–3 washes were

needed and for glucose and glycerol 4–6 washes were need because the producer amount of EPS. The water was recovered in a clean recipient to allow crystals sedimentation by 10 min. The crystals were washed with boiling water until the supernatant became clear. To eliminate the excess of organic residuals, sediment was washed several times with 1:3 acetone-alcohol (HYCEL, Zapopan, México) solution in vortex by 10 sec., until supernatant became clear. The supernatant was thrown out and crystals were oven at 80 °C for 12 h to evaporate the rest of water and solvent.

Petrographic analysis

A petrographic analysis was performed to internally characterize the crystals using polarizing microscopy. Standard petrographic thin section procedures (Murphy 1986) were modified to perform thin section of one fraction of BCC powder and flake aggregates. BCC were encapsulated into clear epoxy resin (COMEX, Mexico City, México) on the flat surface of a standard slide glass (26 × 46 mm). After curing epoxy resin, were trimmed and grinded until reach 100 µm thickness employing a saw/grinder machine (Ingram Thin Section Model 65). Encapsulated samples were finished by hand using silicon carbide and alumina abrasives in order to get ~ 25 µm of thickness and a polished surface. Thin sections were observed in Leica Petrographic Microscope DM2700 P with cross Nicols. The integrity of all samples was first evaluated in bright field (e.g. Fig. S2).

SEM analysis

Other fraction of BCC was sputtered with Pt/Ag layer by cathodic sputtering (MNT-JS1600, Micronano Tools) during 1 min (Folk and Lynch 1997). BCC were observed by Scanning Electron Microscopy (SEM) in a JEOL JSM-7000F Field Emission Scanning Electron Microscope. To determinate crystals elemental composition, Energy Dispersive X-Ray Spectroscopy (EDX) were performed.

XRD analysis

Polymorphism and crystalline structures were determined by X-ray diffraction (XRD) using powder diffraction data method (Kontoyannis 2000). Panalytical X´pert Pro X-Ray MRD diffractometer was used; the X-ray emission was produced by copper cathode at Kα1 = 1.5405 °A wavelength and 20 to 80 2θ degrees by 0.001step protocol. The diffractograms were analyzed by means of the MATCH software.

Crystallite size and crystallinity index determination

The theoretical crystallite size (τ) was calculated using the Scherrer equation (Patterson 1939; Eq. 1), using 0.9 as shape factor (K), the specific wavelength (λ) provide by the XRD equipment, the line broadening half the maximum intensity (β) and the Bragg angle (θ) of the more intense plane of the calcite (104) (Person et al. 1995; Merino and Morales 2008).

$$\tau = \frac{K\lambda}{\beta cos\theta}$$

1

Likewise, the area of the most intense peak (104) was determined, and compared with respect to mineral calcite, which has a crystallinity index (CI) of 99%. The area of (104), (006), (110) and (113) peak was calculated in order to calculate the crystalline index (IC; Eq. 2).

$$IC = \frac{\sum Areaofpeakspattern}{\sum Areaofpeakssample}$$

2

ATR-FTIR analysis

The crystalline and amorphous phases composition was performed by Fourier Transformed Infra-Red spectrometry (ATR-FTIR). Crystals were analyzed in Bruker Alfa Platino-ATR spectrophotometer from 4000 to 400 nm.

Thermal stability

To analyze crystal composition and thermal stability, 5 mg of biogenic crystals were compacted in aluminum pans. An SDT Q600 TA equipment was used for thermogravimetric analysis, temperature range was from 35° to 850° C, heating rate was 10 °C/min, working atmosphere was air at 50 mL/min of gas flow.

Results

Composites biomineralization

After 9 days of incubation at 37º C, *B. subtilis* mineralized colonies were harvested from Petri dishes with nutrient agar supplemented with glycerol + $CaCl_2$ (GLY), glucose + $CaCl_2$ (GLC), calcium lactate (LAC) or calcium acetate (ACE). Colonies formed in GLY and GLC (Fig. 1a and 1b) were scattered distributed over the plate comparatively of LAC or ACE (Fig. 1c and 1d) conditions. Once the material was detached with hot water (~ 90° C), washed and cleaned up from non-mineralized cells and EPS, it was observed at metallographic microscope.

The bigger confluent colonies were obtained in both non-coupled conditions (GLY and GLC), but with irregular forms in GLY (Fig. 1a) than GLC (Fig. 1b); these were orange pigmented too. Coupled conditions showed smaller mineralized colonies, with typical smooth and regular borders; where the saturation of Petri dish was predominantly in ACE condition (Fig. 1d).

Internal structures of biogenic calcium carbonate crystals

A petrographic study was performed in mineralized colonies of *B. subtilis* grown on different media (Fig. 2). The mineral shape, size composite, internal structure, and optical properties were shown in polarizing and analyzed light, where the black background (epoxy resin, Fig. S2) is surrounding Biogenic

Carbonate Crystals (BCC) in bright colors. In GLY condition (Fig. 2a), BBC shown the most amorphous growth habit. All BCC shown at least three interference colors of 4th order in Michel-Lévy scale with wedge-shaped margin, suggesting calcite presence. Moreover, in BCC-LAC and BCC-ACE (Fig. 2c, 2d), it is clear light extinction North-South/Este-West between microscope polarizing axes and mineral axes (Maltese cross), which fits to fiber-radial crystal distribution. BCC-GLC (Fig. 2b) exhibited a better spherical and bigger size composite (~ 300 μm of diameter). Nevertheless, also it can be overbed ring growths of smaller crystals. In all conditions, BCC apparently grown in a layered crystal arrange, although in BCC-GLY (Fig. 2a) mineral layer seems do not have an order in comparison to other obtained crystals. BCC-GLC (Fig. 2b) have a crystal layers starting in several nuclei all over the colony. It can be observed as changes in color separated by color lines. However, for BCC-LAC (Fig. 2c) and BCC-ACE (Fig. 2d), layers start from top to the bottom layer, in that order until forms the crystal. Finally, micrite present botryoidal growth with nodular arrangement in BCC-GLC (Fig. 2b and Fig. S3).

BCC crystalline properties

To determine the crystallographic properties of the BCC produced, the samples were subjected to X-ray diffraction by powder method. Calcite was the only $CaCO_3$ polymorphism obtained in BCC of each condition (Fig. 3a), as was inferred from the intensity of 104 surface plane. The BCC-GLC shown the highest crystallinity (85%), followed by BCC-ACE (80%), BCC-LAC (56.7%) and BCC-GLY (53.4%) (Fig. 3b). The crystallite size interval for all BCC was between 30 to 60 nm, where the largest and smallest one was obtained in BCC-GLC and BCC-LAC, respectively.

Crystalline structures and superficial morphology of BCC

The BCC morphology was analyzed by SEM. BCC aggregates sizes varied in the four growth conditions as follow: 33–217 μm of BCC-GLY; 43–316 μm of BCC-GLC; 48–118 μm of BCC-LAC and 38–172 μm of BCC-ACE.

BCC presented different mineralized structures, such as scales (Fig. 4a) or rhombohedral irregular shapes (Fig. 4c) formed in uncouple and couple calcium-carbon sources, respectively. Those structures correspond to calcite morphology. The mineralized EPS were more evident in BCC-GLY and BCC-GLC (Fig. 4b) than BCC-LAC or BCC-ACE. Crystallite formations were evident just in non-coupled sources (Fig. 4a, 4b and Fig. S4a, S4b); their sizes are in concordance to XRD data (Fig. 3b). In all condition cells were mineralized, INDBM was evident in coupled calcium-carbon sources, where rhombohedral shapes occurred in cell wall (Fig. 4d). The mineralized cells were also observed inside colonies formed in ACE condition (Fig. S5). As well, other ultra-structures were observed between mineralized cells, like fibers growing in nets (0.5 μm) between foliated scales and mineralized EPS of BCC-GLC (Fig. 5a) or forming bridges (10 μm) between colonies in BCC-LAC (Fig. 5a).

BCC composition analysis

The thermogravimetric analysis (TGA) of BCC showed similar patterns in all four conditions (Fig. 6). They presented three important mass lost (Fig. 6a) at 75º C and 237º C and between 700º to 800º C. These changes are more pronounced in BCC-GLY. The first one could be associate to dehydration of amorphous $CaCO_3$. Second one corresponds to organic matter loss, where BCC-GLY reduced its mass 22%, BCC-LAC 6.5%, BCC-GLC 5.5%, and BCC-ACE 5%. The last process belongs to $CaCO_3$ decomposition to CaO on BCC, where in BCC-GLC, BCC-LAC and BCC-ACE the lost occurred between 38.3 to 40.4%. While in BCC-GLY weight lost was 28.8%. These thermic BCC processes (Fig. 6b) could be described as: endothermic one near 100º C, followed by exothermic one between 335º – 340º C, and two endothermic process at 535º C and between 728º – 802º C. The changes in heat flow during thermal decomposition (Fig. 6c) were measured by enthalpy (ΔH). In 331º – 338º C the values were 430.96, 480.73, 579.69, 10497 J g^{-1} $°C^{-1}$, with peak temperature in 332º, 350º, 347.5º and 349º C for BCC-ACE, BCC-LCA, BCC-GLC, and BCC-GLY, respectively. In 744º – 800º C the reported values were 1149.6, 1758.8, 2275.6, 4487.5 J g^{-1} $°C^{-1}$ at 744.38º, 745.74º, 755.64º, 799.99 °C for BCC-GLY, BCC-GLC, BCC-LAC, and BCC-ACE, respectively. The BCC with better and worst thermal stability were obtained in ACE and GLY media, respectively. All data above indicate the presence of higher organic matter in BCC-GLY.

Additionally, EDX analysis of BCC surfaces showed that all composites were mainly formed by C, O, Ca and, in lower proportion by N, P, and S (Fig. S6a). Besides, all BCC were evaluated by FTIR-ATR spectrophotometry in the near infrared spectrum. The absorption bans of CO_3^{-2}-calcite vibrational groups were observed (Fig. S6b), such as $v_{4s}CO_3$, at 712 cm^{-1}, $v_{2as}CO_3$ at 870 cm^{-1} and $v_{3as}CO_3$ at 1409 cm^{-1} (Plav et al., 1999). Moreover, the presence of functional groups of organic origin was found, such as v_{s3} PO_4 at 580 cm^{-1} and v COP at 1145 cm^{-1}; narrowing of -C-O-C- and C-O related to polysaccharides between 1000 to 1154 cm^{-1}; amide and amino groups as $vsNH_2$ at 1623 cm^{-1}; v_s CO at 1653 cm^{-1}; v_s CO^{free} at 1682 cm^{-1}; δNH at 776 cm^{-1} an sulfur group as v_{as} SO at 1390 cm^{-1}. After 1800 cm^{-1}, no signal of a functional group was observed.

Discussion

The BCC produced in presence of *B. subtilis* had different morphological and crystallographic properties, depending of media composition: a) conditions where the calcium source is not associated to carbon one, non-coupled (GYL and GLC); or b) where the calcium is attached to the carbon source, coupled (LAC and ACE). The predominant morphologies in petri dish were mineralized colonies with rounded shape and convex (Fig. 1), in contrast to experiments done in liquid media were dumbbell, rhombohedral and spherulitic shapes are common (Han et al. 2019). Independently to media, the main factor that induced carbonate precipitation is the microenvironment alkalinization, that enhance complexation of Ca^{+2} free ions with free CO_3^{-2} ion (Dupraz et al. 2009). Specifically, in nutrient media, glutamine deamination (Dervaux et al. 2014), and carbonic anhydrase activity (Frankel and Bazylinski 2003; Perito and Mastromei 2011; Oppenheimer-Shaanan et al. 2016; Han et al. 2019) could provoke this pH changes

(Jiménez-Delgadillo et al. 2018). pH changes in long term *Bacillus* culture in agar-rich media (Robinson et al. 1991).

Only BCC-GLC were orange pigmented (Fig. 1b), which is related to iron chelation by pulcherriminic acid produced in biofilms of carbohydrates supplemented media (Arnaouteli et al. 2019).

Thin section micrography show birefringence phenomena under polarized light (Fig. 2). However, due the presence of optical interference color of light green-extinction characteristic 4th order birefringence it can be interrelated has arrangement of typical calcite carbonate crystals (Aizenberg and Hendler 2004). However, did not show the characteristic calcite cleavage. Difference in the interference color in crystals indicates a non-oriented arrangement of microcrystal growth, it can be produced by the randomized growth of bacteria colonies. However, mineral growth in glycerol media is also determined by crystal nucleation in EPS produced by cells (Oppenheimer-Shaanan et al. 2016), that is probably the cause of its amorphous habit. Micrite is common in marine sediments and microbialites (Perri and Spadafora 2011) with spherical and radial-fibers growth as we observed in all BCC; mineralized cells are also present (Rasmussen and Muhling 2019).

Several strains of *Bacillus* could mineralize different polymorphisms of $CaCO_3$, such calcite and vaterite (Seifan et al. 2016; Andrei et al. 2017; Huynh et al. 2017), but factors that induce only one kind of polymorphism are not jet understood. In this work well only observe calcite production, even if calcium-carbon source was non-coupled. Other authors have identified this crystalline phase in *B. subtilis* (Zhuang et al. 2018; Han et al. 2019). The obtained BCC had different crystallinity (BCC-GLY < BCC-ACE < BCC-LAC < BCC-GLC), possibly related to mineralization process in each formation-condition (Fig. 3b). The IC of BCC-GLC may be similar to abiotic process pH, Ca^{2+} concentration and nucleation sites are critical (Perito and Mastromei 2011). For coupled calcium-carbon sources, like ACE (Fig. 4d, S5), the mineralization mainly occurred over cellular structures such as cell wall and EPS (Marvasi et al. 2012; Dhami et al. 2013). In that sources, critical Ca^{2+} concentration could be accumulated in cell wall because the efflux pump and specific channels (Saier et al. 2002). The membrane and cell wall components could be nucleation sites because its negative charges of teichoic acid that attract Ca^{2+} (Perito et al. 2014).

Lower IC in BCC-LAC and BCC-GLY could be associated to higher production of organic matter or amorphous calcium carbonate (ACC). This is the polymorphic precursor of crystalline structures under biotic or abiotic mineralization (Bots et al. 2012; Cantaert et al. 2016). Some interaction with glycoproteins or organic molecules increased the ACC stability and prevent spontaneous crystallization (Aizenberg et al. 2002; Weiner et al. 2003). Additionally, in non-coupled calcium-carbon sources (GLY and GLC), BCC nanodeposites with the same sizes of calculate crystallite were evident over calcite scales and mineralized EPS (Fig. 4a, 4b, S4). This is the first work where such kind of precipitants are observed in biocomposites of *B. subtilis*.

The main components of *B. subtilis* EPS, that promote calcite aggregation, are TasA and TapA amyloid proteins and exopolysaccharides (Azulay et al. 2019); moreover, there are reports of nanotubes formation

when *B. subtilis* grows in rich media (Bhattacharya et al. 2019). In this study, both structures were observed in BCC-GLC (Fig. 5b) and BCC-LAC (Fig. 5c), respectively.

In order to understand the BCC composition, TGA and DSC analysis were performed (Fig. 6). Thermic change of biotic and abiotic vaterite was reported with an exothermic peak between 317º – 318º C, that was associated to organic matter decomposition with CO_2 and NO_2 release (Rodriguez-Navarro et al. 2007). Furthermore, at 700º – 800º C a second reaction occurs, from $CaCO_3$ to CaO (Al Omari et al. 2016). As we saw, BCC-GLY presented greater abundance of organic matrix; however, temperature decomposition not follow enthalpy rise. Some organic acids could change temperature peaks of that process (Li et al. 2018).

Mineralization degree (BCC-ACE > BCC-LAC > BCC-GLC > BCC-GLY) also affected thermic stability of BCC in relation to enthalpy and decomposition temperatures (Fig. 6). This may be to mineral abundance or lattice variation (Pokroy et al. 2006), such as in BCC-GLC with higher crystallinity but low presence of $CaCO_3$.

In BCC, EPS could increase complexation by the interaction of the ions with the electronegativity charge of its expose functional groups (Ercole et al. 2007; Oppenheimer-Shaanan et al. 2016). This explain the random nucleation of minerals that occurs in the bacteria microenvironment. However, in BCC-GLY the synthesis level of EPS increases the amount of nucleation sites but affected negatively the crystallinity. EPS have a key role in $CaCO_3$ precipitation (Arias and Fernández 2008), and *B. subtilis* produce high amount of different types in glycerol supplemented media (Oppenheimer-Shaanan et al. 2016). Besides, EPS is important to $CaCO_3$ precipitation (Decho 2010; López-Moreno et al. 2014), because it attract Ca^{2+} to its chemical functional groups, such as: COO-, NH_3-, PO_4- and SO_4- groups (Schmitt and Flemming 1998; Humbert and Quilès 2011). Those group, related to main EPS components (exoplysaccharides and proteins) play a key role in BCC formation (Azulay et al. 2018). P content may be related to extracellular DNA usually present in EPS (Peng et al. 2020).

In this study the BCC produced in presence of *B. subtilis* were constituted manly by calcite. We demonstrated that the quality of this biogenic calcite was only influenced by calcium-carbon source. In that sense, the best composites were obtained when bacteria were grown in supplemented medium by glucose and calcium chloride. Finally, this non-coupled calcium-carbon condition promotes several nucleation sites for $CaCO_3$ precipitation, and it was no need to provide with urea to achieve the necessary alkalinity.

Abbreviations

B. subtilis, *Bacillus subtilis*; BCC, biogenic carbonate crystals; GLY, glycerol + $CaCl_2$; GLC, glucose + $CaCl_2$; LAC, calcium lactate; ACE, calcium acetate; OM, organic matter; ACC, amorphous calcium carbon; CBM, controlled biological mineralization; INDBM, induced biological mineralization; INFBM, influenced biological mineralization; EPS, extracellular polymeric substances; SEM, Scanning Electron Microscopy;

EDX, Energy Dispersive X-Ray Spectroscopy; XRD, X-ray diffraction; CI, crystallinity index; ATR-FTIR, Fourier Transformed Infra-Red spectrometry; TGA, Thermogravimetric; DSC, differentia scanning calorimetry.

Declarations

Ethics approval:

This article does not contain any studies with human participants or animals performed by any of the authors.

Consent for publication:

Not applicable

Conflict of Interest:

The authors declare that they have no conflict of interest.

Availability of data and materials

All relevant data are within the manuscript and its Supplementary Material, file 1.

Funding:

This research was financially supported by Universidad Autónoma de Ciudad Juárez.

Authors' contributions

Planning and designing of this study: MAR; performing the experiments: HFP; performing the data analysis: HFP, MAR, BAT, AIP and MGG; manuscript drafting: HFP, MAR, MGG, BAT and AIP. All authors read and approved the final manuscript.

Acknowledgments

This work represents part of Héctor Ferral-Pérez's PhD thesis done in "Programa de Doctorado en Ciencias Químico Biológicas" at UACJ with a scholarship grant of CONACyT. We acknowledge to Eng. Montserrat Hernández Ramírez from "Laboratorio de Geología", IIT-UACJ. for her advice in petographyc

techniques; to M. C. Hortencia Reyes Blas from “Laboratorio de Microscopía Avanzada” and Tech. Ivan Salcido from “Centro de Investigación en Ciencia y Tecnología Aplicada”, IIT-UACJ for SEM thechnical assistant; to M. C. Lorena Herrera from “Instituto de Ingeniería y Tecnología” at UACJ, for XRD technical assistant; to M. C. Marco Antonio Leiva, from Cinvestav-IPN, for Match software training; to PhD. Erasto Armando Zaragoza Contreras from Termic Analysis Laboratory at “Centro de Investigación en Materiales Avanzados” (CIMAV, Chihuahua), for TGA and DCC analysis. FTIR equipment was kindly lended by PhD. Yobani Reyes López from “Laboratorio de Materiales Híbridos Nanoestructurados”, ICB-UACJ.

References

1. Aizenberg J, Hendler G (2004) Designing efficient microlens arrays: lessons from Nature. J Mater Chem 14:2066
2. Aizenberg J, Lambert G, Weiner S, Addadi L (2002) Factor involved in the formation of amorphous and crystalline calcium carbonate: A study of an ascidian skeleton. J Am Chem Soc 124:32–39
3. Al Omari M, Rashid I, Qinna N, Badwan AA (2016) Calcium Carbonate. In: Brittain. HG (ed) Profiles of Drug Substances, Excipients and Related Methodology. Burlington, pp 31–132
4. Andrei AS, Pausan MR, Tamas T, Har N, Barbu-Tudoran L, Leopold N, Banciu HL (2017) Diversity and biomineralization potential of the epilithic bacterial communities inhabiting the oldest public stone monument of Cluj-Napoca (Transylvania, Romania). Front Microbiol 8:1–13
5. Arias J, Fernández M (2008) Polysaccharides and proteoglycans in calcium carbonate – based biomineralization. Chem Rev 108:4472–4482
6. Arnaouteli S, Matoz-Fernandez DA, Porter M, Kalamara M, Abbott J, MacPhee CE, Davidson FA, Stanley-Wall NR (2019) Pulcherrimin formation controls growth arrest of the *Bacillus subtilis* biofilm. Proc Natl Acad Sci U S A 116:13553-13562
7. Azulay DN, Chai L (2019) Calcium Carbonate Formation in the Presence of Biopolymeric Additives. J Vis Exp. 147
8. Banks ED, Taylor NM, Gulley J, Lubbers BR, Giarrizo JG, Bullen HA, Hoehler TM, Barton HA (2010) Bacterial calcium carbonate precipitation in cave environments: A function of calcium homeostasis. Geomicrobiol J 27:444–454
9. Barabesi C, Galizzi A, Mastromei G, Rossi M, Tamburini E, Perito B (2007) *Bacillus subtilis* gene cluster involved in calcium carbonate biomineralization. J Bacteriol 189:228–235
10. Bhattacharya S, Baidya AK, Pal RR, Mamou G, Gatt YE, Margalit H, Rosenshine I, Ben-Yehuda S (2019) A Ubiquitous Platform for Bacterial Nanotube Biogenesis. Cell Reports 27:334–342
11. Bots P, Benning L, Rodriguez-Blanco J, Roncal-Herrero T, Shaw S (2012) Mechanistic Insights into the Crystallization of Amorphous Calcium Carbonate (ACC). Cryst Growth Des 12:3806–3814
12. Cantaert B, Kuo D, Matsumura S, Nishimura T, Sakamoto T, Kato T (2016) Use of Amorphous Calcium Carbonate for the Design of New Materials. ChemPlusChem 82:107–120

13. Ciferri O, Tiano P, Mastromei G (2000) Of microbes on art. The role of microbial communities in the degradation and protection of cultural heritage. Springer US, Boston
14. De Vrij W, Bulthuis R, Postma E, Konings WN (1985) Calcium transport in membrane vesicles of *Bacillus subtilis*. J Bacteriol. 164:1294–1300
15. Decho AW (2010) Overview of biopolymer-induced mineralization: What goes on in biofilms? Ecol Eng 36:137–144
16. Dervaux J, Magniez JC, Libchaber A (2014) On growth and form of *Bacillus subtilis* biofilms. Interface Focus 4: 20130051
17. Dhami NK, Reddy MS, Mukherjee A (2014) Synergistic Role of Bacterial Urease and Carbonic Anhydrase in Carbonate Mineralization. Appl Biochem Biotechnol 172:2552–2561
18. Dhami NK, Reddy MS, Mukherjee A (2013) Biomineralization of calcium carbonates and their engineered applications: a review. Front Microbiol 4:19–25
19. Dove PM, Weiner S, Yoreo JJ De (2003) Biomineralization. Mineralogical Society of America Geochemical Society, Washington, D. C.
20. Dupraz C, Reid RP, Braissant O, Decho AW, Norman RS, Visscher PT (2009) Processes of carbonate precipitation in modern microbial mats. Earth-Science Rev 96:141–162
21. Ercole C, Cacchio P, Botta AL, Centi V, Lepidi A (2007) Bacterially induced mineralization of calcium carbonate: the role of exopolysaccharides and capsular polysaccharides. Microsc Microanal 13:42–50
22. Frankel RB, Bazylinski DA (2003) Biologically induced mineralization by bacteria. Rev Mineral Geochemistry 54:95–114
23. Folk R, Lynch F (1997) The possible role of nanobacteria (Dwarf bacteria) in clay–mineral diagenesis and the importance of careful sample preparation in high-magnification SEM study. J Sediment Res 67:583–589
24. Han Z, Wang J, Zhao H, Tucker M, Zhao Y, Wu G, Zhou J, Yin J, Zhang H, Zhang X, Yan H (2019) Mechanism of Biomineralization Induced by *Bacillus subtilis* J2 and Characteristics of the Biominerals. Minerals 9(218):1–25
25. Humbert F, Quilès F (2011) In-situ study of early stages of biofilm formation under different environmental stresses by ATR-FTIR spectroscopy. In: Mendes-Vilas A (ed) Science against microbial pathogens: Communicating current research and technological advances, 1st ed. Formatex Research Center, pp 889–895
26. Huynh NNT, Hung PV, Sangadji S, Son NK (2018) Identify the microbial-induced calcium carbonate precipitation in seawater environment and autogenous healing of microbial-modified mortar. SEATUC Symp 11:1–5
27. Jiménez–Delgadillo R, Valdés–Rodríguez SE, Olalde–Portugal V (2018) Effect of pH and temperature on the growth and antagonistic activity of *Bacillus subtilis* on *Rizoctonia solani*. Rev Mex Fis 36:256–275

28. Knorre H v., Krumbein WE (2000) Bacterial Calcification. In: Microbial Sediments. Springer Berlin Heidelberg, Berlin, Heidelberg, pp 25–31
29. Kontoyannis C G, Vagenas N V (2000) Calcium carbonate phase analysis using XRD and FT-Raman spectroscopy. Analyst 125:251–255
30. Li XG, Lv Y, Ma BG, Wang WQ, Jian SW (2017) Decomposition kinetic characteristics of calcium carbonate containing organic acids by TGA. Arabian J Chem 10:S2534-S2538
31. López-Moreno A, Sepúlveda-Sánchez JD, Alonso Guzmán EM, Le Borgne S (2014) Calcium carbonate precipitation by heterotrophic bacteria isolated from biofilms formed on deteriorated ignimbrite stones: influence of calcium on EPS production and biofilm formation by these isolates. Biofouling 30:547–60
32. Marvasi M, Casillas-Santiago LM, Henríquez T, Casillas-Martinez L (2017) Involvement of *etfA* gene during $CaCO_3$ precipitation in *Bacillus subtilis* biofilm. Geomicrobiol J 34:722–728.
33. Marvasi M, Gallagher KL, Martinez LC, Molina Pagan WC, Rodríguez Santiago RE, Castilloveitía Vega G, Visscher PT (2012) Importance of B4 Medium in Determining Organomineralization Potential of Bacterial Environmental Isolates. Geomicrobiol J 29:916–924
34. Meier A, Kastner A, Harries D, Wierzbicka-Wieczorek M, Majzlan J, Büchel G, Kothe E (2017) Calcium carbonates: induced biomineralization with controlled macromorphology. Biogeosciences 14:4867–4878
35. Merino L, Morales J (2008) Relationship of the cristallinity index (CI) with the age and content of Fe and CO_3 ions in vertebrate fossil samples. Estud Geol 64:75–87
36. Micallef R, Vella D, Sinagra E, Zammit G (2016) Biocalcifying *Bacillus subtilis* cells effectively consolidate deteriorated Globigerina limestone. J Ind Microbiol Biotechnol 43:941–952
37. Murphy C P (1986) Thin section preparation of soils and sediments. Berkhamsted: A.B. Academic
38. Ngwenya BT (2016) Bacterial Mineralization. In: Reference Module in Materials Science and Materials Engineering. Elsevier
39. Oppenheimer-Shaanan Y, Sibony-Nevo O, Bloom-Ackermann Z, Suissa R, Steinberg N, Kartvelishvily E, Brumfeld V, Kolodkin-Gal I (2016) Spatio-temporal assembly of functional mineral scaffolds within microbial biofilms. npj Biofilms Microbiomes 2:15031
40. Patterson A (1939) The Scherrer Formula for X-Ray Particle Size Determination. Phys Rev 56:978–982
41. Páramo L A, Narváez J A, Ortega-Morales B O (2015) La bioprecipitación de carbonato de calcio por la biota nativa como un método de restauración. Nexo Rev Cient 28:25–40
42. Peng N, Cai P, Mortimer M, Wu Y, Gao C, Huang Q (2020) The exopolysaccharide-eDNA interaction modulates 3D architecture of *Bacillus subtilis* biofilm. BMC Microbiol 20:115
43. Perito B, Biagiotti L, Daly S, Galizzi A, Tiano P, Mastromei G, Ciferri O, Editor, G Mastromei PT, O. Ciferri and G Mastromei PT (2000) Bacterial genes involved in calcite crystal precipitation. Microbes Art role Microb communities Degrad Prot Cult Herit, pp 219–230

44. Perito B, Mastromei G (2011) Molecular Basis of Bacterial Calcium Carbonate Precipitation. Prog Mol Subcell Biol 52:113–139
45. Perito B, Marvasi M, Barabesi C, Mastromei G, Bracci S, Vendrell M, Tiano P (2014) A *Bacillus subtilis* cell fraction (BCF) inducing calcium carbonate precipitation: Biotechnological perspectives for monumental stone reinforcement. J Cult Herit 15:345–351
46. Perri E, Spadafora A (2011) Evidence of microbial biomineralization in modern and ancient stromatolites. In: Tewari, V, Seckbach J (Eds) STROMATOLITES: Interaction of microbes with sediments.1 edn, Springer
47. Person A, Bocherens H, Saliège J-F, Paris F, Zeitoun V, Gérard M (1995) Early Diagenetic Evolution of Bone Phosphate: An X-ray Diffractometry Analysis. J Archaeol Sci 22:211–221
48. Plav B, Kobe S, Orel B (1999) Identification of crystallization forms of $CaCO_3$ with FTIR spectroscopy. Kovine Zlitine Teh 33:517–521
49. Pokroy B, Fitch A, Marin F, Kapon M, Adir N, Zolotoyabko E (2006) Anisotropic lattice distortions in biogenic calcite induced by intra-crystalline organic molecules. J Struc Biol 155:96–103
50. Priya JN, Kannan M, Priyanka P, Mary SV (2016) A Study on Characterization of EPS and Media Optimization for Bacterial Calcium Carbonate Precipitation. Int J Curr Microbiol Appl Sci 5:590–595
51. Rasmussen B, Muhling, JR (2019) Organic-rich microfossils produced by oil infiltration of hollow silicified bacteria: Evidence from the ca. 340 Ma Red Dog Zn-Pb deposit, Alaska. Geol 47:1107–1111
52. Reeksting BJ, Hoffmann TD, Tan L, Paine K, Gebhard S (2020) In-depth profiling of calcite precipitation by environmental bacteria reveals fundamental mechanistic differences with relevance to application. Appl Environ Microbiol 86:e02739-19
53. Robinson TP, Wimpenny JWT, Earnshaw RG (1991) pH gradients through colonies of *Bacillus cereus* and the surrounding agar. J Gen Microbiol 137:2885–2889
54. Rodriguez-Navarro C, Jimenez-Lopez C, Rodriguez-Navarro A, Gonzalez-Muñoz MT, Rodriguez-Gallego M (2007) Bacterially mediated mineralization of vaterite. Geochim Cosmochim Acta 71:1197–1213
55. Rusznyák A, Akob D, Nietzsche S, Eusterhues K, Totsche KW, Neu TR, Frosch T, Popp J, Keiner R, Geletneky J, Katzschmann L, Schulze ED, Küse K (2012) Calcite Biomineralization by Bacterial Isolates from the Recently Discovered Pristine Karstic Herrenberg Cave. Appl Environ Microb 78:1157–1167
56. Saier MH Jr, Goldman SR, Maile RR, Moreno MS, Weyler W, Yang N, Paulsen IT (2002) Transport capabilities encoded within the *Bacillus subtilis* genome. J Mol Microbiol Biotechnol 4:37-67.
57. Schmitt J, Flemming H-C (1998) FTIR-spectroscopy in microbial and material analysis. Int Biodeterior Biodegradation 41:1–11
58. Seifan M, Samani A, Berenjian A (2016) Induced calcium carbonate precipitation using *Bacillus* species. Appl Microbiol Biotechnol 100:9895–9906

59. Shirakawa MA, Cincotto MA, Atencio D, Gaylarde CC, John VM (2011) Effect of culture medium on biocalcification by *Pseudomonas putida*, *Lysinibacillus sphaericus* and *Bacillus subtilis*. Brazilian J Microbiol 42:499–507
60. Sierra-Beltran MG, Jonkers HM, Schlangen E (2014) Characterization of sustainable bio-based mortar for concrete repair. Constr Build Mater 67:344–352
61. Stumm W (1990) Aquatic chemical kinetics: reactions rates in natural waters. 1st ed.
62. Weiner S, Levi-Kalisman Y, Raz S, Addadi L (2003) Biologically Formed Amorphous Calcium Carbonate. Connect Tissue Res 44:214–218
63. Zhuang D, Yan H, Tucker ME, Zhao H, Han Z, Zhao Y, Suna B, Lia D, Panb J, Zhaoa Y, Menga R, Shanb G, Zhanga X, Tang R (2018) Calcite precipitation induced by *Bacillus cereus* MRR2 cultured at different Ca^{2+} concentrations: Further insights into biotic and abiotic calcite. Chem Geol 500:64–87

Figures

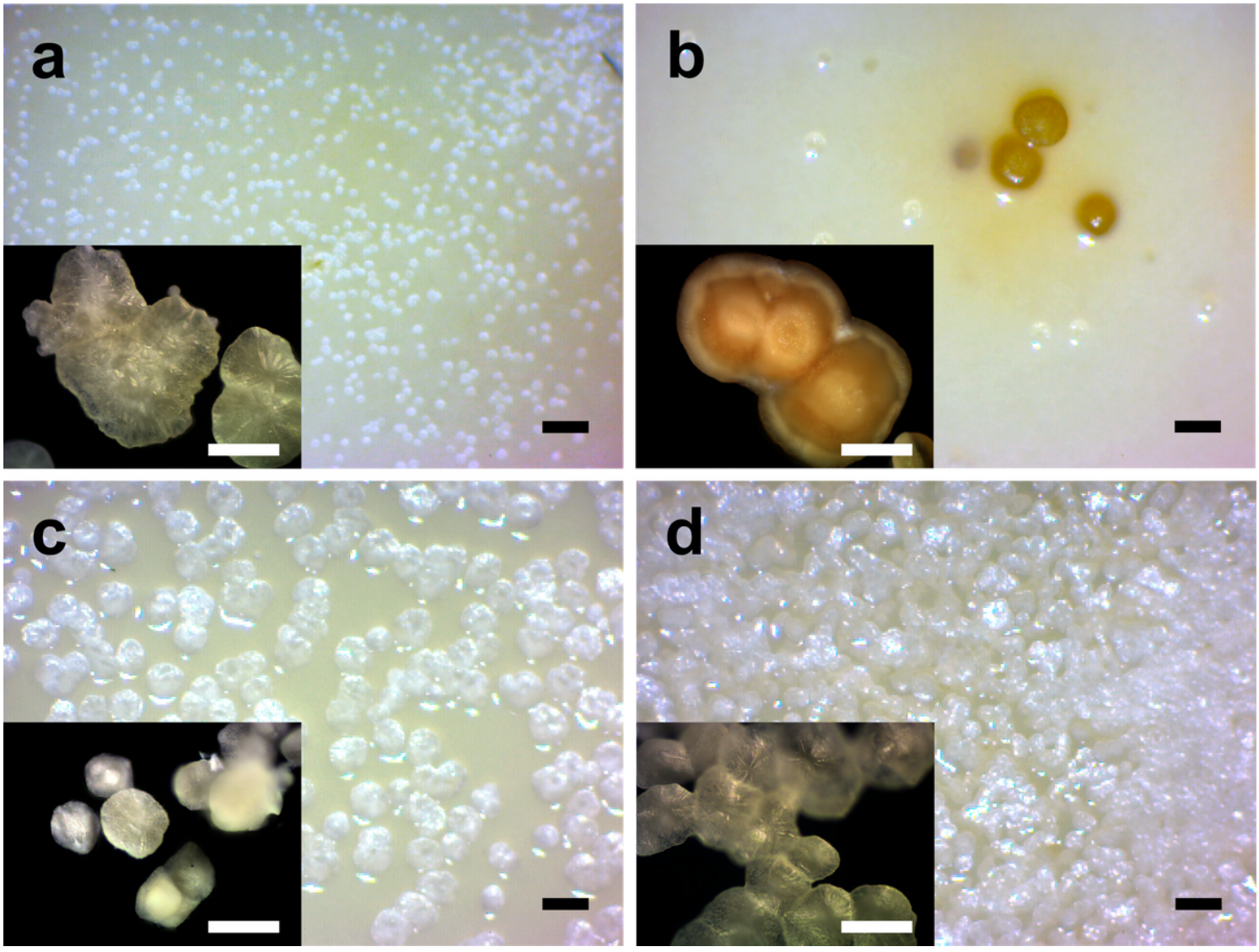

Figure 1

Cultures of B. subtilis and mineralized cell colonies formed in coupled and non-coupled calcium-carbon sources media. Images show stereoscopic view of plates and metallographic micrographs of recovered composites from (a) GLY, (b) GLC, (c) LAC, and (d) ACE media. Scale bars: 1 mm (black); 100 µm (white).

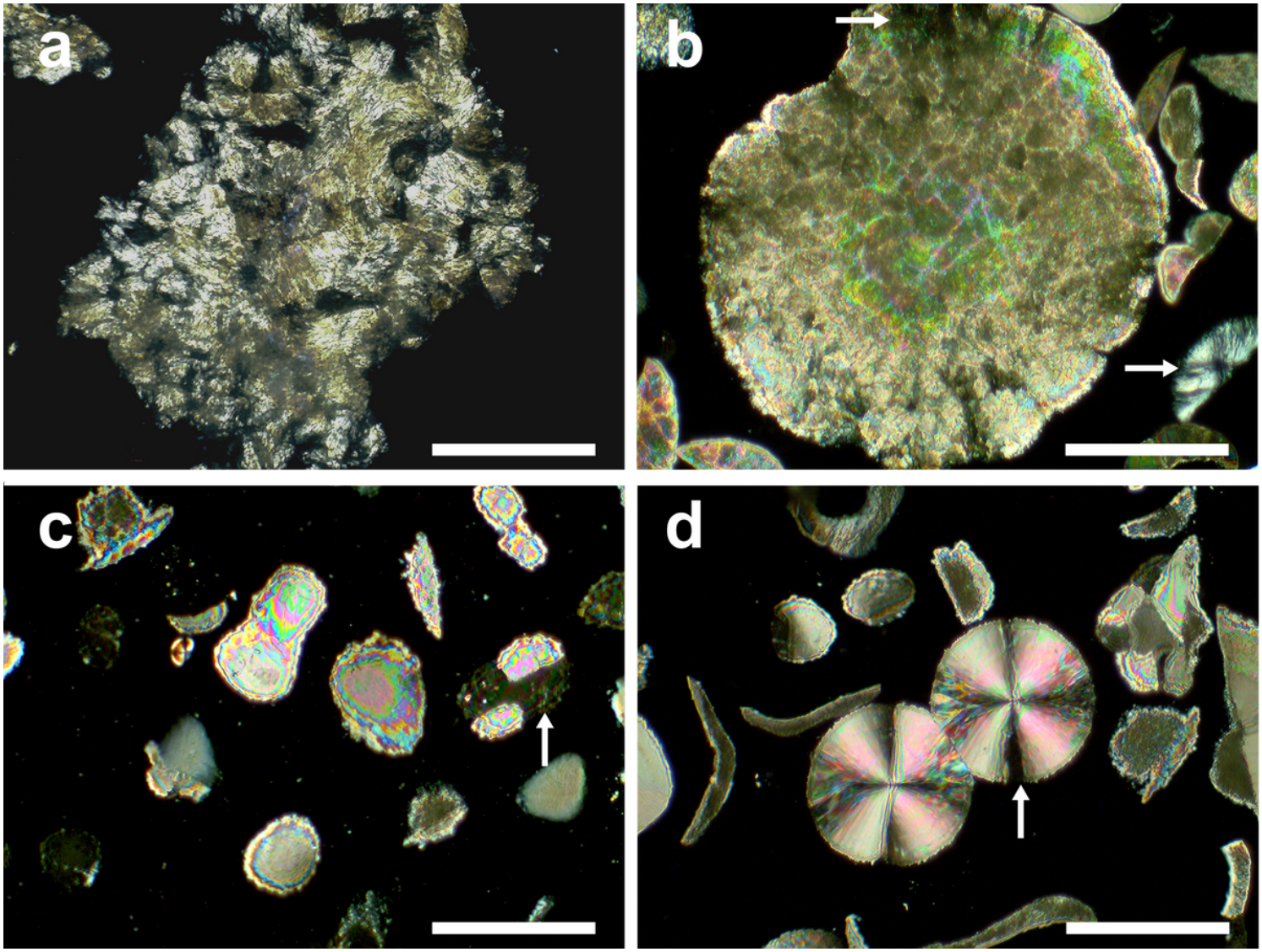

Figure 2

Thin section micrographs of mineral grow composites produced in presence of Bacillus subtilis at different condition. (a) BCC-GLY, (b) BCC-GLC, (c) BCC-LAC, and (d) BCC-ACE. Images were acquired with polarized and analyzed light. They show size, shape, and optical properties of biogenetic crystals from diverse media. Arrows symbol show a key optical property, of light extinction (see result and discussion text). Scale bar: 100 µm.

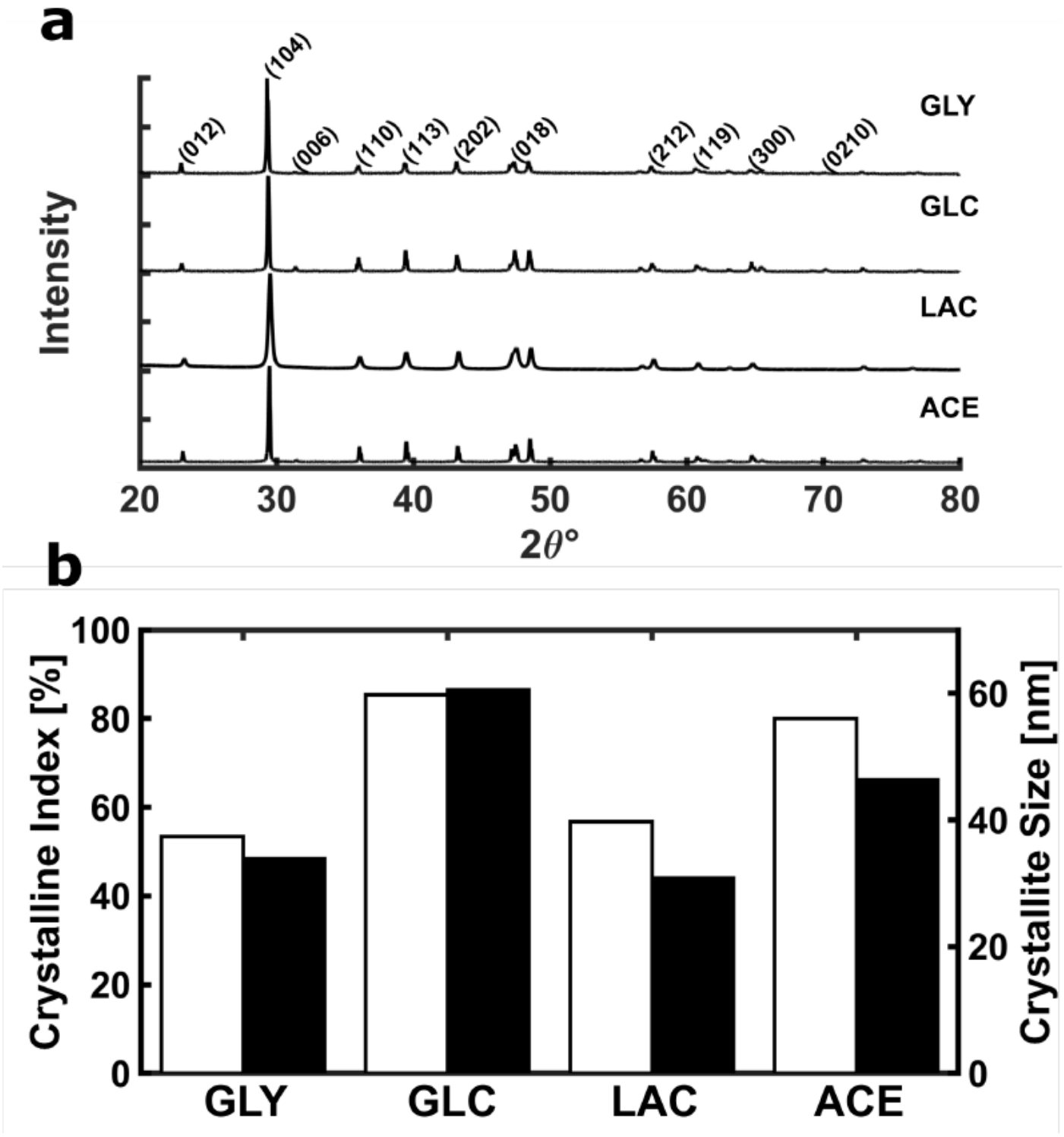

Figure 3

Crystallographic properties of BCC. Diffractogram (a) of BCC-GLY, BCC-GLC, BCC-LAC and BCC-ACE. (b) Bars show the crystallinity index (white, left scale) and crystallite size of 104 peak (black, right scale) of composites obtained in each condition.

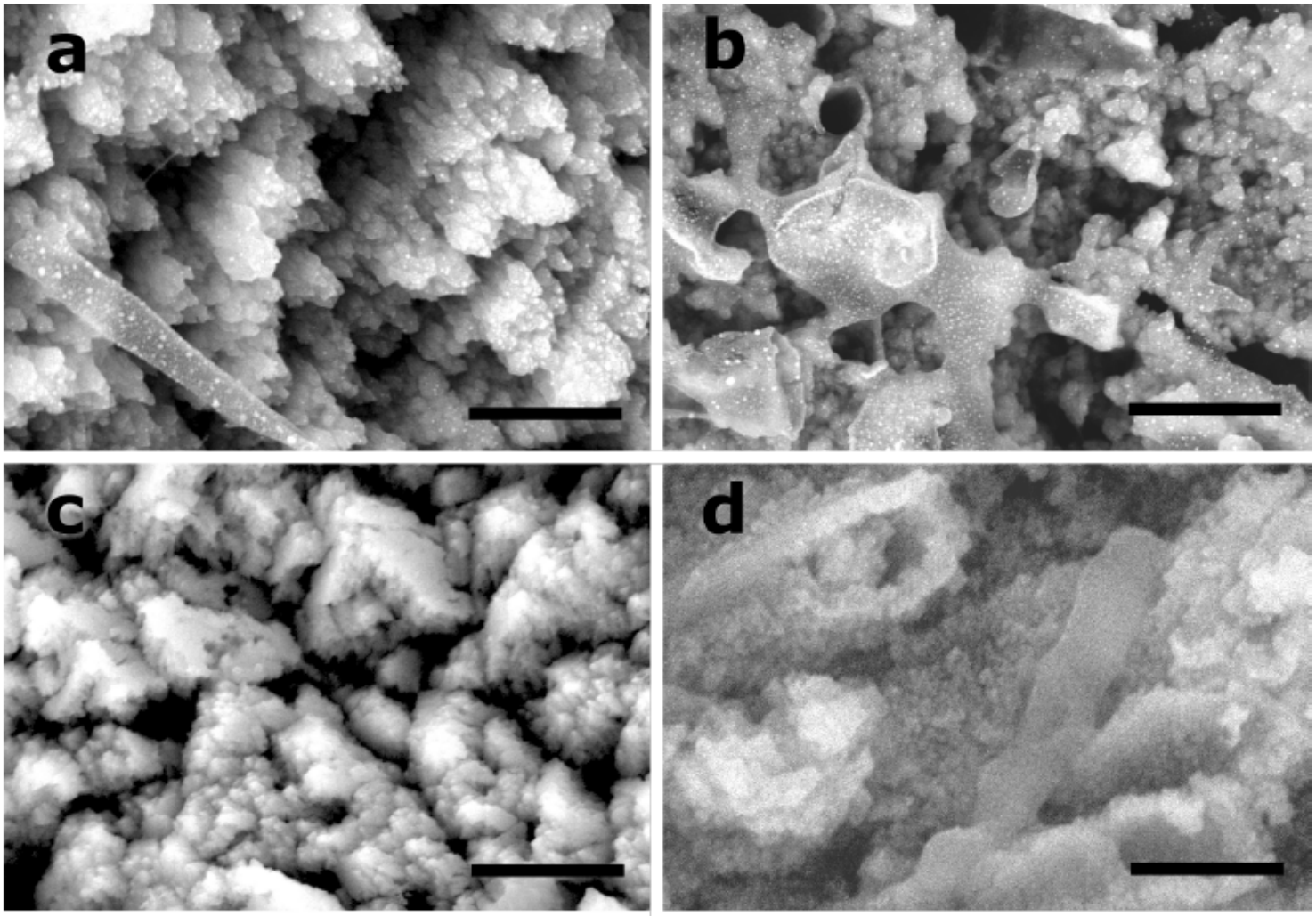

Figure 4

BCC structures formed in non-coupled and coupled calcium-carbon sources. SEM images of BCC-GLC (a, c) and BCC-ACE (c, d) are shown. Scales (a) and rhombohedral calcite irregular shapes (c) are present. Crystallites grow over calcite aggregates and mineralized EPS in non-coupled sources (a, b). Besides, induced mineralization occurs over the cell wall in coupled source (d). Scale bars: 1 μm.

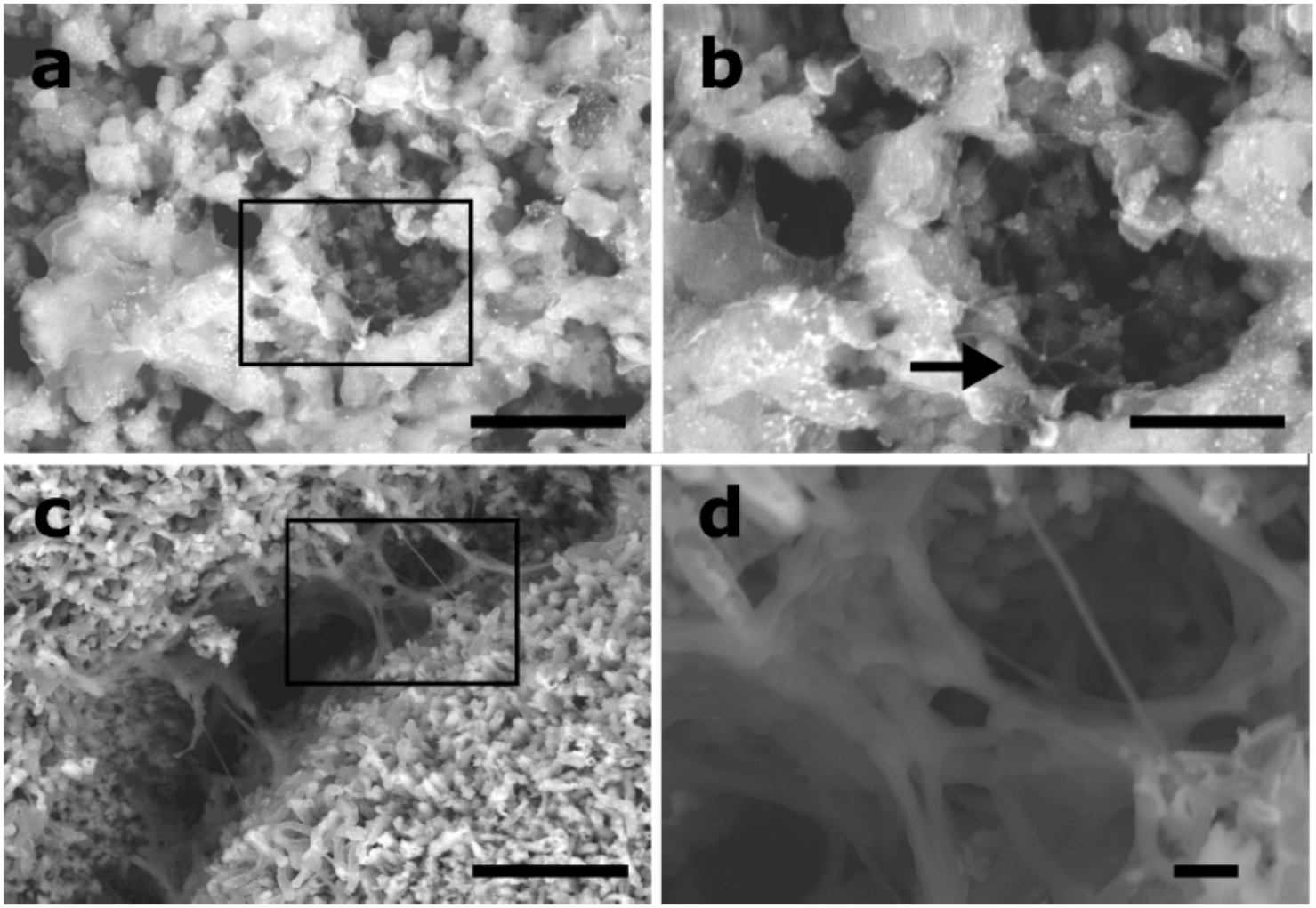

Figure 5

Mineralized micro and nanofibers of BCC-EPS. SEM images of (a) BBC-GLC and (c) BCC-LAC are shown. The rectangles (b, d) indicate its respective magnifications, and nanofibers are pointed out (black arrow). Scale bars: 10 μm (a) and 1 μm (b), and 1 μm (c) and 0.5 μm (d).

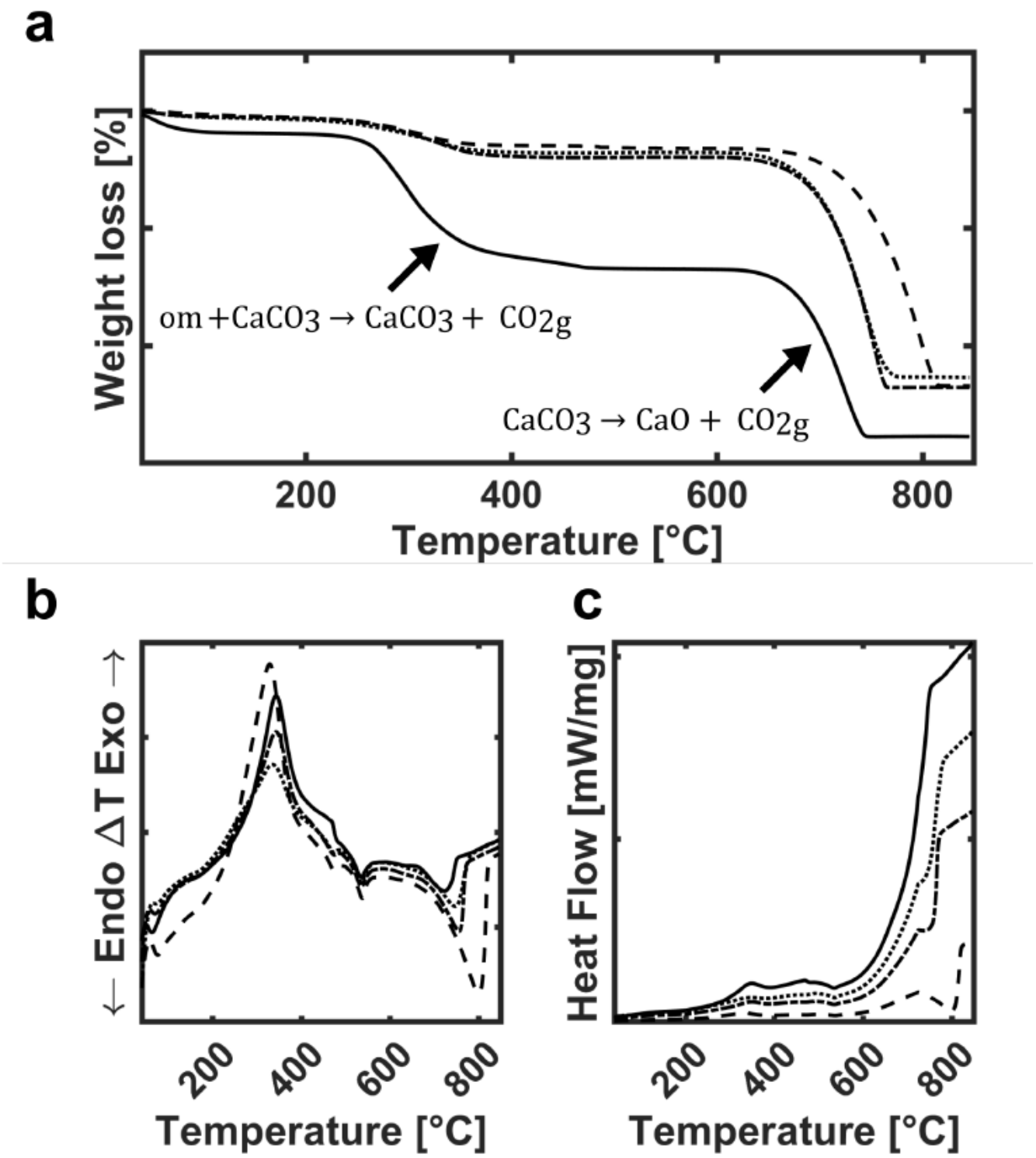

Figure 6

Phase transition of composites formed on different media. (a) Thermogravimetric (TGA) profile and material weight loss of organic matrix (om), carbon dioxide (CO2) and calcium oxide (CaO). (b) Differential thermal analysis and (c) differentia scanning calorimetry (DSC) show degradation enthalpy and crystalline transition of amorphous calcium carbonate (ACC) to crystalline CaCO3. Lines indicate BCC-GLY (solid), BCC-GLC (dot), BCC-LAC (grid), and BCC-ACE (dashed).

Supplementary Files

This is a list of supplementary files associated with this preprint. Click to download.

- SupplementaryESM1AMBEFerralPerez.docx